

# COMPUTATIONAL MODELING OF FLUID-STRUCTURE INTERACTION USING FINITE ELEMENT METHOD UNDER ALE FORMULATIONS APPROACH

Carlos Eduardo da Silva, kadu@lamce.coppe.ufrj.br

Nestor Oscar Guevara, guevara@lamce.coppe.ufrj.br

José Ricardo P. Gonzalez, jrpgonzalez@gmail.com

José Luis Drummond Alves, jalves@lamce.coppe.ufrj.br

Laboratory for Computational Methods in Engineering, COPPE/UFRJ

**Abstract.** *The simulation of Fluid structure interaction is becoming of great importance for industry, in particular in naval engineering for vortex-induced vibrations (VIV) and analysis of the sloshing impact load on the tank of ships. There are several approaches for solving a fluid structure interaction problem. The classical one is the Lagrangian formulation for the structure and arbitrary Lagrangian Eulerian (ALE) formulation for fluid, a fluid structure interface is defined between the fluid and the structure may be treated with volume of fluid (VOF) formulation. This work is concerned with the modeling of the interaction of fluid flow with moving structures, are presented algorithms under ALE and VOF approach to compute the complete set of actions between the fluid and the structure. Numerical applications are presented in particular VIV problem.*

**Keywords:** *Arbitrary Lagrangian Eulerian Formulations, Fluid-Structure Interaction, vortex-induced vibrations*

## 1. Introduction

The variety of FSI problems scenarios is abundant and ranges from parachutes and airbags flows to blood flow in arteries and riser interference for a deep water riser array presents a complex ocean engineering problem. The optimization of engineered systems involved on those problems through the intensive use of computer simulation as physical modeling and, according to the desired accuracy, the solution can be quite expensive. Computer modeling of such situations faces important difficulties and is supposed to reunite three main aspects: accuracy (reproducing the main physical mechanisms present), robustness (stability of the involved algorithms leading to convergence) and computational performance (matching the needs of the applications). The main computational challenges related to such highly nonlinear problem are determining the evolution of the interfaces location and solving the coupled multi-fluid-structure interaction problem. There are a large number of numerical methods devoted to the computation of a single fluid interacting with structures or free-surface problems. In the problem of a single fluid interacting with structures, moving mesh methods, within the framework of the Arbitrary Lagrangian-Eulerian (ALE) formulation or space-time deforming domain methods, are usually preferred, specially when the structures might undergo large motions. The amount of work describing ALE methods is enormous, and we do not intend here to present a literature review, we rather refer the interested reader to books and recent paper collections [Donea e Huerta, 2003] and papers addressing particular aspects of the overall methodology [Farhat et al., 2010, Dettmer e Peric, 2006]. These references are all related to finite elements, addressing a variety of topics, such as discretization methodologies for fluids and structures, moving meshes and adaptivity, coupling strategies etc.

In the present work we extend the simulation capabilities of the solver introduced in [Elias et al., 2009], including robust general mesh movement strategies and rigid body dynamics. Staggered, or also known as partitioned, algorithms provide an interesting approach to handle such coupled problems as they allow to explore methods designed to treat the physics of each sub-system in an optimal way. Moreover, they also permit to put together tested high performance numerical codes already developed, even if they consist of black-boxes, the data structures used in different modulus of the code can be easily made compatible. Such convenient features come at a price, those algorithms are usually only conditional stable in contrast with monolithic approaches. Monolithic algorithms, in which all equations are solved at the same time for each time step, become less attractive for the type of problems we have in mind as the computational cost for solving the coupled system grows nonlinearly with the number of variables. As no general theory has been proposed for those staggered algorithms, their robustness and stability characteristics might be investigated through numerical tests. The focus here is to report the integration of the several solution components and present the resulting staggered algorithm, which has been implemented in its simplest form, as no sub-iteration, often used to improve stability. The numerical examples presented here that deal with important prototypes of the situations of interest has shown no stability issues.

The remainder of this paper is organized as follows. Next section discusses the governing equations for the free-surface flow, mesh movement and rigid body dynamics. The resulting staggered time marching algorithm and the finite element components for the fluid flow solver and mesh movement are also briefly reviewed. Section 3 presents some development

and verification examples. First we investigate the robustness of the mesh movement scheme when the resulting system of linear equations is solved by an iterative driver. A riser interference problem is solved to demonstrate the present FSI flow capabilities. The paper ends with a summary of our main conclusions.

## 2. Governing equations

### 2.1 Incompressible Fluid Flow

Let  $\Omega \subset \mathfrak{R}^{n_{sd}}$  be the spatial domain, where  $n_{sd}$  is the number of space dimensions, let  $\Gamma$  denote the boundary of  $\Omega$  and the interval  $[0, t_f]$  denote the time domain of the problem. We consider the following convective form of the Navier-Stokes equations governing the incompressible flows of two immiscible fluids that uses a reference frame provided by the ALE formulation which are defined over the space-time domain  $\Omega \times [0, t_f]$ :

$$\rho \left( \frac{\partial \mathbf{u}}{\partial t} + (\mathbf{u} - \mathbf{u}_{mesh}) \cdot \nabla \mathbf{u} - \mathbf{b} \right) - \nabla \cdot \sigma = \mathbf{0}, \quad (1)$$

$$\nabla \cdot \mathbf{u} = 0, \quad (2)$$

where  $\rho$  and  $\mathbf{u}$  are the density and velocity,  $\mathbf{u}_{mesh}$  is the reference frame velocity, The latter, in the context of a Finite Element approximation, is taken as the velocity of the vertices of the discrete mesh, which gives room for accommodating the coupling of fluid and solid motions and adapt the mesh for describing the flow considering the new relative position of the solid body. Moreover,  $\mathbf{b}$  represents the body force vector carrying the gravity acceleration effect and the Cauchy stress tensor  $\sigma$  for a incompressible Newtonian fluid is given as:

$$\sigma(p, \mathbf{u}) = -p\mathbf{1} + 2\mu\mathbf{D}(\mathbf{u}), \quad (3)$$

where  $p$  is the pressure,  $\mathbf{1}$  is the identity tensor,  $\mu$  is the dynamic viscosity and  $\mathbf{D}$  is the rate-of-deformation tensor defined as

$$\mathbf{D}(\mathbf{u}) = \frac{1}{2} \left( \nabla \mathbf{u} + (\nabla \mathbf{u})^T \right). \quad (4)$$

In the present work a large eddy simulation (LES) approach to turbulence is considered by the use of a classic Smagorinsky turbulence model [Smagorinsky, 1963]. In this model, the viscosity  $\mu$  is augmented by a subgrid-scale viscosity  $\mu_{SGS}$  proportional to the norm of the local rate-of-deformation tensor and to a filter width  $h$  defined here as the cubic root of the element volume,

$$\mu_{SGS} = \rho(C_S h)^2 |2\mathbf{D}(\mathbf{u}) : \mathbf{D}(\mathbf{u})|, \quad (5)$$

where  $C_S$  is the Smagorinsky constant, taken as 0.1.

The essential and natural boundary conditions associated with Eqs. (1) and (2) can be imposed at different portions of the boundary  $\Gamma$  and represented by,

$$\mathbf{u} = \mathbf{u}_E \quad \text{on } \Gamma_E \quad (6)$$

$$\mathbf{u} = \dot{\mathbf{d}}_L \quad \text{on } \Gamma_L \quad (7)$$

$$\mathbf{n} \cdot \sigma = \mathbf{h} \quad \text{on } \Gamma_h \quad (8)$$

where  $\Gamma_E$  is the Eulerian boundary of the fluid with essential boundary condition,  $\Gamma_L$  is the Lagrangian boundary, i.e., the moving (rigid) body surface,  $\Gamma_h$  is the boundary with applied traction forces and  $\mathbf{n}$  is the unit outward normal vector to  $\Gamma_h$ . The fields  $\mathbf{u}_E$   $\dot{\mathbf{d}}_L$  are respectively the fluid velocity applied in the Eulerian boundary and the fluid-structure interface displacements. Eq. (7) establishes which interface is considered as non-slip conditions.

The boundaries  $\Gamma_L$ ,  $\Gamma_E$ ,  $\Gamma_h$  and  $\Gamma$  are related by:

$$\Gamma_g = \Gamma_E \cup \Gamma_L \quad (9)$$

$$\Gamma = \Gamma_g \cup \Gamma_h \quad (10)$$

Accordingly with the type of flows to be analyzed, here involving free surfaces, the model can be stated within a two fluids (A and B) point of view. Therefore the spatial domain  $\Omega = \Omega_A \cup \Omega_B$  is split into two regions; one corresponding to the space occupied by the original fluid and the second an arbitrary region containing part of the air surrounding this fluid. Both fluids are separated by means of a moving internal interface  $\Gamma_{int}(t)$ , not known a priori. The position of the interface is computed taking into the consideration that velocities and the traction vectors for both fluids assume the same value on this interface ( $\mathbf{u}_A = \mathbf{u}_B$ ;  $\sigma_A \cdot \mathbf{n}_{int} = \sigma_B \cdot \mathbf{n}_{int}$ ), where  $\mathbf{n}_{int}$  is the unit normal vector to interface  $\Gamma_{int}$ . Note that this last condition only holds if surface tension between fluids is negligible.

### 3. Mesh movement

There are many options available for addressing node repositioning in ALE frameworks. For instance, an elasticity operator in an ancillary boundary value problem BVP for repositioning nodes, is employed in [Johnson e Tezduyar, 1994]. In this work, our choice is the scheme proposed for 3D applications in [Masud et al., 2007], where nodes are repositioned as result of the solution of a scalar BVP, Eqs (11)-(13), written on  $\Omega \times [0, t_f]$ :

$$\nabla \cdot ([1 + \tau] \nabla) d_i = 0 \quad i = 1, \dots, n_{sd}, \quad (11)$$

$$\mathbf{d} = \mathbf{d}_L \quad \text{on } \Gamma_L, \quad (12)$$

$$\mathbf{d} = \mathbf{0} \quad \text{on } \Gamma - \Gamma_L \quad (13)$$

where,  $\tau = \tau(\mathbf{x}, t)$  is a artificial diffusivity,  $\mathbf{d}$  are the nodal displacements in the ALE step for each spatial coordinate,  $\mathbf{d}_L$  is the vector of nodal displacements already defined in the previous section.

A Galerkin variational formulation is used to solve the mesh BVP. The self-adjoint operator in Eq. (11) and its discrete form render a symmetric set of algebraic equations of the global form:

$$\mathbf{K}(\tau)\mathbf{d} = \mathbf{r} \quad (14)$$

where  $\mathbf{K}$  and  $\mathbf{r}$  are the global matrix and the forcing term which contains the restriction  $\mathbf{d}_L$ , respectively.

Once having solved the BVP Eqs. (11)-(13), mesh velocity appearing in Eq. (1) can be computed by:

$$\mathbf{u}_{mesh} = \frac{\mathbf{d}(\mathbf{x}, t)}{\Delta t} \quad (15)$$

where  $\Delta t$  is the time-step size.

The heterogeneous artificial diffusivity is computed for each element of the mesh, i.e.  $\tau(\mathbf{x}, t) = \tau^e(t)$  according to:

$$\tau^e = \frac{1 - V_{min}/V_{max}}{V^e/V_{max}} \quad (16)$$

where  $V_{min}$ ,  $V_{max}$  are, respectively, the least and the largest volume for the elements in the mesh, and  $V^e$  is the the current element volume. The artificial diffusivity (16) have the crucial role of stiffening the elements in the immediate neighborhood of the body, allowing mesh distortion in the far field where large elements are usually located. The quality of the tetrahedral meshes updated by this method can be evaluated using the following metrics:

$$Q_e = \frac{72\sqrt{3}}{\left(\sum_{i=1}^6 l_i^2\right)^{3/2}} V^e \quad (17)$$

where  $l_i$  are the edges of the element. We also used a relative metric given by:

$$Q_{rel}^{t_n} = \frac{Q_e^{t_n}}{Q_e^{t_0}} \quad (18)$$

### 4. Fluid structure interaction

Nodal forces equivalent (in equilibrium) with the full stress, measured in the surrounding elements, can be computed by:

$$\mathbf{f}_{int}^e = \int_{\Omega_e} \mathbf{B}^T \sigma d\Omega \quad (19)$$

where the tensor  $\sigma$  was defined in Eq. (3),  $\Omega_e$  is the element domain, and  $\mathbf{B}$  is given by:

$$\mathbf{B} = B_{jI} = \frac{\partial N_I}{\partial x_j}, \quad I = 1, \dots, n_{en} \quad (20)$$

where  $N_I$  are the shape functions of an element and  $n_{en}$  is the number of element nodes. Evaluation of integral (19) is only required for those elements meeting the condition:

$$\Omega_e \subset Adj(\Gamma_L) \quad (21)$$

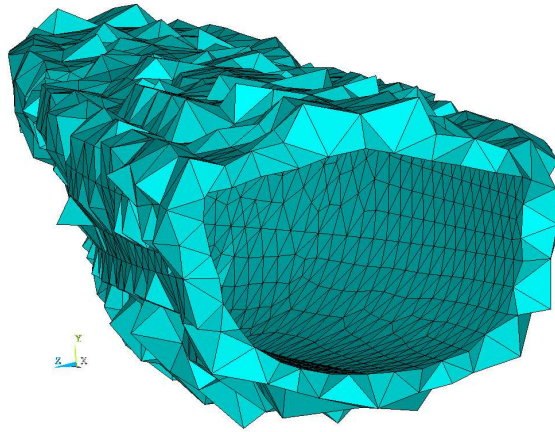


Figure 1. Portion of the elements attached to a Lagrangian boundary in a ship hull model

where  $Adj(\Gamma_L)$  is the region spanning elements with at least one node lying in  $\Gamma_L$ , as illustrated in Fig. (1) for a ship hull mesh, that is, elements adjacent to  $\Gamma_L$ .

Thus, the resulting forces on the immersed body can be computed by the sum of each element internal force contribution (computed as equivalent nodal forces). Note that elements adjacent to  $\Gamma_L$  may be on the wet or non-wet portion of the immersed body. The fluid properties assigned to each element by the VOF method defines the proper contributions to the element internal forces, that is,

$$\mathbf{f}_n = \mathbf{A}_e \mathbf{f}_{int}^e |_{\Gamma_L^e} \quad (22)$$

where

$$\Gamma_L^e = \Gamma_L \cap \Gamma^e \quad (23)$$

in which  $\Gamma^e$  is the boundary of  $\Omega_e$  and the assembly operator  $\mathbf{A}_e$  is used here instead of the ordinary sum symbol to denote the finite element assembly process.

The resultant of the hydrodynamic forces on the body, required in Eq.(26), is then given by:

$$\mathbf{f} = - \sum_{n=1}^{nb} \mathbf{f}_n \quad (24)$$

where the summation is taken as the assembling operator for the elements contribution,  $\mathbf{f}_n$ , computed from Eq. (22) for all  $nb$  nodes in  $\Gamma_L$ . Finally, the resulting moment acting in the rigid body mass center is computed as:

$$\mathbf{m} = \sum_{n=1}^{nb} \mathbf{r}_n \times \mathbf{f}_n \quad (25)$$

where  $\mathbf{r}_n$  is the position vector of each node in  $\Gamma_L$  with respect to the mass center of the rigid body.

## 5. Rigid body dynamics

In this work the immersed or partially immersed structures are considered to undergo rigid body motions, that are conveniently described by the usual 6 (six) degrees of freedom (3 displacements and 3 rotations) referred to its center of mass. Body weight and the hydrodynamic forces acting on the body's surface are summed-up as resulting forces and moments referred to the center of mass. These hydrodynamic forces are evaluated based on the fields  $(\mathbf{u}, p)$ , using the full stress tensor given by Eq. (3). The motion of the rigid body's mass center governs the motion of every mesh node in  $\Gamma_L$ , as "master-slave" kinematic constraints throughout the analysis.

The rigid body motion is governed by the Newton-Euler equations:

$$m\mathbf{a} = \mathbf{f} + m\mathbf{g} \quad (26)$$

$$\mathbf{I}_b \dot{\boldsymbol{\omega}} + \boldsymbol{\omega} \times \mathbf{I}_b \boldsymbol{\omega} = \mathbf{m} \quad (27)$$

where  $m$  is the mass of the body,  $\mathbf{I}_b$  is the tensor of inertia of the body referred to its mass center, computed with respect to an reference system attached to the body, hence  $\mathbf{I}_b$  is constant for all time, as shown in [?, ?]. The vectors  $\mathbf{a}$  and  $\dot{\omega}$  are the translation and angular acceleration of the body, respectively, with respect to an stationary reference system. Finally  $\mathbf{f}$  and  $\mathbf{m}$  are the resulting forces and torques acting on the body, due to the fluid interaction with the body's surface, already shown in (24) and (25), respectively.

For time integration of the system formed by Eqs. (26) and (27) we use an approach proposed in [?] and reported in [Formaggia et al., 2008], where the velocity is available by an explicit two-step Adam-Bashforth scheme,

$$\mathbf{v}^{n+1} = \mathbf{v}^n + \frac{\Delta t}{2m} \cdot (3\mathbf{f}^n - \mathbf{f}^{n-1}) \quad (28)$$

and the translation components are obtained using a Crank-Nicholson implicit operator, as follows:

$$\mathbf{x}^{n+1} = \mathbf{x}^n + \frac{\Delta t}{2} (\mathbf{v}^{n+1} + \mathbf{v}^n). \quad (29)$$

Analogously, a scheme similar to Eqs. (28) and (29) is applied to the Euler Eq. (27), except for two additional intermediary steps. First, an inversion of the inertia matrix, recalling the solution of (27) for  $\dot{\omega}$  according to:

$$\dot{\omega} = \mathbf{I}_b^{-1} (\mathbf{m} - \omega \times \mathbf{I}_b \omega) \quad (30)$$

and in a second step, we define the vector:

$$\bar{\mathbf{m}}^n = (\mathbf{m}^n - \omega^n \times \mathbf{I}_b \omega^n). \quad (31)$$

Finally, the angular velocity and rotation of the body are updated according to:

$$\omega^{n+1} = \omega^n + \frac{\Delta t}{2} \mathbf{I}_b^{-1} (3\bar{\mathbf{m}}^n - \bar{\mathbf{m}}^{n-1}) \quad (32)$$

$$\theta^{n+1} = \theta^n + \frac{\Delta t}{2} (\omega^{n+1} + \omega^n) \quad (33)$$

## 6. Coupling Solver

To advance in time the solution we solve sequentially for the rigid body position, update the mesh, solve for flow and free surface position, computing wet and non wet portions of the rigid body, as shown in *Algorithm 1*. This algorithm accommodates easily subiterations between the different fields and predictor-corrector procedure, which may extend the stability range of simple staggered schemes [X, Y, Z] in single fluid FSI computations. Here, with the need to solve for the VOF marker, we introduce an additional field and in this case it is not clear the effects of subiterations or predictor-corrector procedures.

*Algorithm 1:*  
Given  $(\mathbf{u}, p, \phi)$  in  $t = t_0$  set  $\mathbf{u}_{mesh}(\mathbf{x}, t_0) = \mathbf{0}$   
Loop in time ( $t_n$ )

1. compute equivalent nodal forces for elements with at least one node lying in  $\Gamma_L$ , Eq. (22)
2. compute resulting forces and moments referred to the body's mass center MC, Eq. (24)-(25)
3. compute body motion, Newton-Euler equations for new position, Eqs. (28)-(29) and (32)-(33)
4. use an updated Lagrangian description for the rigid body defining displacements of MC
5. apply the rigid, master-slave kinematic constraints used to describe rigid body motion of nodes in  $\Gamma_L$
6. solve for mesh repositioning, a Dirichlet BVP in each coordinate, Eqs. (11)-(13)
7. compute instantaneous mesh velocity, Eq. (15)
8. solve the flow equations incompressible Navier-Stokes in ALE framework  $(\mathbf{u}, p, \mathbf{u}_{mesh})$
9. solve the VOF equations and update the free surface position

End loop in time

According to some authors (see, for example [Felippa et al., 1999, Lohner et al., 2006]), our strategy is similar to a two-way coupling of the *fully explicit partitioned* type, also known by Conventional Sequential Staggered CSS scheme, where the FSI problem is dealt with a change of kinematic and dynamic boundary conditions between the fluid and the rigid body. Our method coupled the effects of fluid flow on the body and their subsequent interactions are taken by a consistent procedure for evaluating the hydrodynamic forces acting on the body and it also ensures continuity in the boundary conditions at the interface. In what follows, our basic assumption is that the matrix of Eq. (14) is available in the previous time step  $t_{n-1}$  the mesh does not move significantly between subsequent timesteps, and the distance from the bodies to an individual nodal point in its neighborhood does not change considerably.

It should be noted that, to the extent of the problems addressed, the physics involved and their space and time resolutions, no instability issues were observed in all simulations below. Extensions of more involved variants of the present FSI algorithm remain to be explored.

## 7. Test cases

In our continuing verification and validation effort of the present implementation, this section addresses three problems. The first problem addresses an usual problem that can be faced in offshore oil production facilities: a two-riser configuration exposed to cross-flow so to observe wake induced oscillations and vortex induced vibrations in the system. For validation, is presented the second problem models a falling sphere on a calm free surface at rest, for which many experimental results are available in literature for assessment of the solution.

### 7.1 Riser Interference

This model problem addresses the behavior of an array of two vertical cylinders, i.e. risers, immersed and exposed to a cross-flow stream, in tandem configuration with respect to the stream. It simulates the interaction between the cylinders and was tailored to show many of the phenomena observed in practice such as vortex induced vibrations (VIV), vortex shedding, wake induced oscillations (WIO), etc. Problem geometry can be described as a box with dimensions  $l=15.0\text{m}$ ,  $h = 10.0\text{m}$ ,  $w=5.0\text{m}$  for length, height and width, respectively. From the bottom up to the top, two identical rigid cylinders (0.50 m in diameter, thickness 0.025m and spaced center-to-center 1.00 m) are fully immersed and positioned at 3.0 m from the inlet boundary surface. The discrete model comprises 177,623 tetrahedral elements and 32,154 nodal points. Figure 2 displays a longitudinal cutaway view of the mesh. Velocity profile was set at inlet boundary so to provide

Reynolds number,  $Re=100$ , according to model dimensions and fluid viscosity. The maximum inexact-Newton tolerance was set to 0.1 while the fixed GMRES tolerance for the advection equation was 0.001.

Boundary conditions for the risers were set as follows: the riser located upstream is fixed and the downstream riser is free to displace sideways. This simulation was run for  $t_f = 1000.0s$  with constant time-step  $\Delta t = 0.005s$ .

Figures 4 and 5 display sequence of snapshots of the simulation showing the motion of the downstream riser, swaying sideways with respect to the upstream riser; color fringes stand for velocity magnitudes.

For a convenient analysis of these results, we should recall Eqs. (3), (22) and (24) and recast (19) as:

$$\mathbf{f} = \mathbf{f}_p + \mathbf{f}_{vis} \tag{34}$$

i.e., the forces acting over the body can be decomposed according to a pressure contribution,  $\mathbf{f}_p$  and a viscous contribution  $\mathbf{f}_{vis}$ .

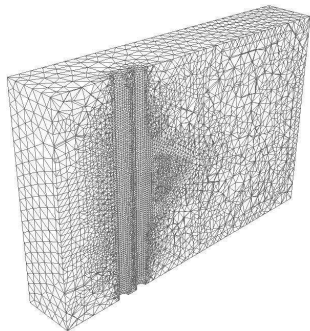


Figure 2. Mesh cutaway view

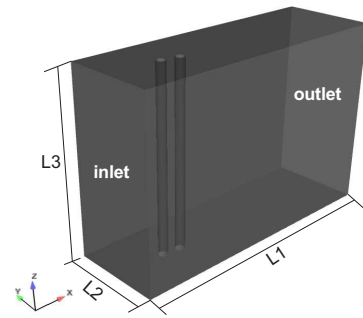


Figure 3. riser-domain

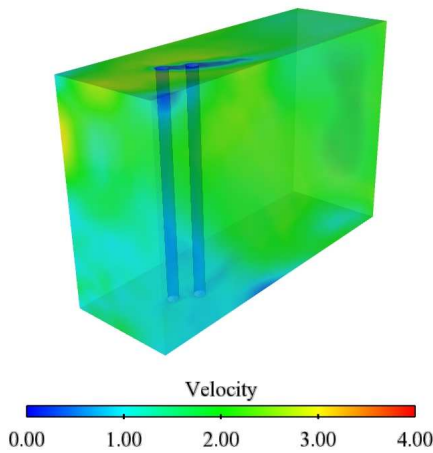


Figure 4. Snapshot for  $t=278.45$  s

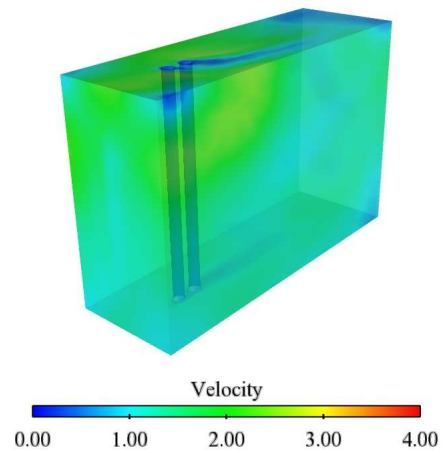


Figure 5. Snapshot for  $t=811.03$  s

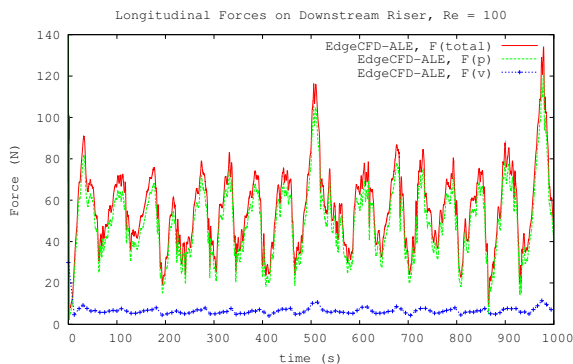


Figure 6. Drag force for downstream riser

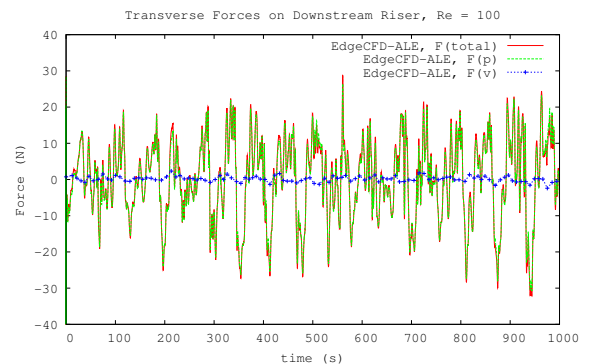


Figure 7. Lift force for downstream riser

Figures 6 and 7 present, respectively, longitudinal (drag) and transverse (lift) forces computed for the downstream riser along with their pressure and viscous components. The results indicate that the viscous component is around 5% of the pressure component, in good agreement with the observations reported in [Fox e McDonald, 1998], in the range around  $Re=100$ .

### 7.2 Validation Test: Falling Sphere

This model problem is relevant to the study of 3D slamming forces on ship falling in pitch motion, for instance, onto the free surface. This problem models a solid sphere free falling vertically onto the surface of a body of fluid initially at rest. Sphere diameter is 0.0572 m, material density is  $\rho=7850.0 \text{ kg/m}^3$  and gravity is  $9.81 \text{ m/s}^2$ . The fluids properties are:  $\rho_{water}=1000.0 \text{ kg/m}^3$ ,  $\mu_{water}=0.01 \text{ kg/(m.s)}$ ,  $\rho_{air}=1.0 \text{ kg/m}^3$  and  $\mu_{air}=0.001 \text{ kg/(m.s)}$ . Tolerances for the incompressible flow and for the VOF marker solvers are set as in the previous example. This simulation run for  $t_f=0.6 \text{ s}$  with constant time-step  $\Delta t=0.001 \text{ s}$ .

The simulation reproduces and compares results with the experiments conducted in [Lavery, 2003], that uses high speed photography to capture the inception of splash, cavity formation and track sphere position in time. The analysis run in parallel, using 8 processors. Figure 8 shows the overall model dimensions. The used mesh comprises 232,282 elements and 40,228 nodes. Figure 9 displays a detail of the free-surface configuration clearly showing the ripples formed at the inception of splash. Figure 10 displays the cavity developed in the free-surface behind the sphere, a few seconds after the splash. Regarding this feature, the angles measured in the numerical simulation and in the reported experiment agree very well. Figure 11 displays a comparison between computed and experimental results regarding vertical position of the sphere after splashing the surface. As can be observed there is good agreement between the results up to 0.55 s. Afterwards, the sphere gets too close to the bottom of the model, rendering an overly distorted mesh, most likely causing the difference between the results.

Figure 12 shows time-histories for several quantities of interest recorded in the simulation. Some of these quantities are also reported in the experimental measurements [Lavery, 2003]. At time  $t = 0$  the vertical position is  $z = 0.60 \text{ m}$ , force and velocity are zero and vertical acceleration is 1.0, which has been normalised with respect to the acceleration of gravity  $g = 9.81 \text{ m/s}$ . It takes only 0.35 s for the sphere to reach the free surface, where the vertical velocity is at its maximum ( $v_z = -3.43 \text{ m/s}$ ). At the inception of splash, vertical force and acceleration reach peak values for a short interval of 0.05 s.

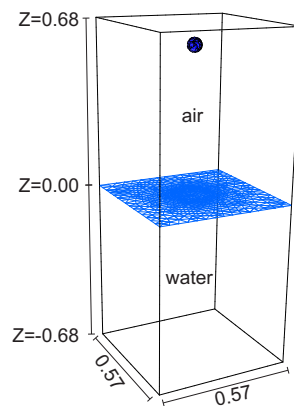


Figure 8. Falling sphere on free surface at rest: overall dimensions and general view of the model (elements for fluid and air are suppressed)

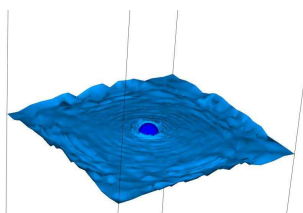


Figure 9. Detail of the free surface at the inception of splash

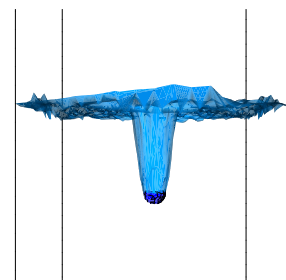


Figure 10. cavity formed at the free surface behind the sphere

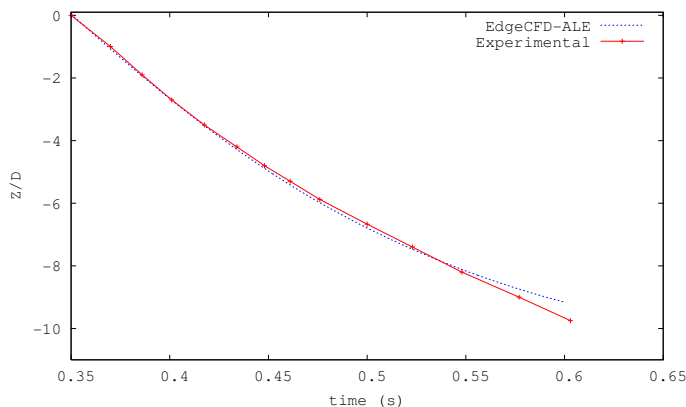


Figure 11. Validation Test: Comparison of numerical and experimental time histories of vertical position

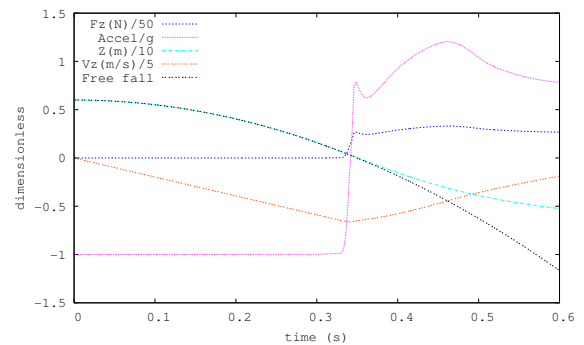


Figure 12. Time history of sphere position ( $Z$ ), vertical force ( $F_z$ ), vertical acceleration ( $Accel_z$ ), vertical velocity ( $V_z$ ) and free-fall position

## 8. Conclusions

In this work we have described FSI solver for offshore hydrodynamics and reported our verification and validation efforts. This solver is designed to profit from a highly efficient parallel edge-based stabilized finite element flow solver that handles free-surface flow problems. The new features incorporated to handle FSI problems inherits these capabilities. The solution of a riser interference is a prototype simulations of situations of interest in offshore hydrodynamics. In this problem results agree well with available results. Although the FSI algorithm is simple, no stability issues have been observed in these examples. Extensions of more involved variants of the present FSI algorithm remain to be explored.

## 9. ACKNOWLEDGEMENTS

The authors acknowledge the financial support of Petrobras, The Petroleum National Agency (ANP, Brazil), MCT/CNPq and FAPERJ. The High Performance Computer Center and the Laboratory for Computational Methods in Engineering at COPPE, The Federal University of Rio de Janeiro provided the computational resources.

## 10. REFERENCES

- Dettmer, W. Peric, D., 2006. Robust and provably second-order explicit-explicit and implicit-explicit staggered time-integrators for highly non-linear compressible fluid-structure interaction problems. *Computer Methods in Applied Mechanics and Engineering*, vol. 195, n. 1, pp. 5754–5779.
- Donea, J. Huerta, A., 2003. *Finite Elements in Flow Problems*. Wiley.
- Elias, R. N., Jr, M. A. G., Coutinho, A. L. G. A., Esperanca, P. T. T., Martins, M. A. D., Ferreira, M. D. A. S., 2009. Free-surface flow simulation using stabilized edge-based finite element methods. In *ASME 28th International Conference on Offshore Mechanics and Arctic Engineering OMAE 2009*, Honolulu, Hawaii.
- Farhat, C., Rallu, A., Wang, K., Belytschko, T., 2010. Robust and provably second-order explicit-explicit and implicit-explicit staggered time-integrators for highly non-linear compressible fluid-structure interaction problems. *International Journal for Numerical Methods in Engineering*, vol. 84, n. 1, pp. 73–107.
- Felippa, C. A., Park, K. C., Farhat, C., 1999. Partitioned analysis of coupled mechanical systems. *Center for Aerospace Structures*, , n. 1, pp. 1–28.
- Formaggia, L., Miglio, E., Mola, A., Parolini, N., 2008. Fluid-structure interaction problems in free-surface flows: Application to Boat dynamics. *International Journal for Numerical Methods in Fluids*, vol. 56, pp. 965–978.
- Fox, R. McDonald, A. T., 1998. *Introduction to Fluid Dynamics*. John Wiley & Sons.
- Johnson, A. A. Tezduyar, T. E., 1994. Mesh updates strategies in parallel finite element computations of flow problems with moving boundaries and interfaces. *Computer Methods in Applied Mechanics and Engineering*, vol. 119, pp. 73–94.

Lavery, S. M., 2003. Experimental Hydrodynamics of Spherical Projectiles Impacting On a Free Surface Using High Speed Imaging Techniques.

Lohner, R., Cezral, J. R., , Yang, C., Baum, J. D., Mestreau, E. L., Soto, O., 2006. Extending the range and applications of the loose coupling approach for fsi simulations. *Lecture Notes in Computational Science and Engineering - Fluid Structure Interaction*, vol. 53, pp. 82–100.

Masud, A., Bhanabhagvanwala, M., Khurram, R. A., 2007. An adaptive mesh rezoning scheme for moving boundary flows and fluid-structure interaction. *Computers and Fluids*, vol. 36, pp. 77–91.

Smagorinsky, J., 1963. General Circulation Experiments with the Primitive Equations.